Microstructural and electrochemical properties of impregnated $La_{0.4}Sr_{0.6}Ti_{0.8}Mn_{0.2}O_{3\pm d}$ into a partially removed Ni SOFC anode substrate

Sung Hun Woo [a,b], Seung-Wook Baek [c], Dae Soo Park [a], Kyeong Eun Song [a], Harald Schlegl [d], Jun-Young Park [e], Jung Hyun Kim [a,*]

[a] Department of Advanced Materials Science and Engineering, Hanbat National University, 125, Dongseodae-Ro, Yuseong-Gu, Daejeon, 34158, Republic of Korea

[b] Energy and Environmental Division, Korea Institute of Ceramic Engineering and Technology (KICET), 101, Soho-Ro, Jinju-Si, Gyeongsangnam-Do, 52851, Republic of Korea

[c] Interdisciplinary Materials Measurement Institute, Korea Research Institute of Standards and Science (KRISS), 267, Gajeong-Ro, Yuseong-Gu, Daejeon, 34113, Republic of Korea

[d] Engineering Department, Lancaster University, Bailrigg, Lancaster LA1 4YW, United Kingdom

[e] HMC, Department of Nanotechnology and Advanced Materials Engineering, Sejong University, 209, Neungdong-Ro, Gwangjin-Gu, Seoul, 05006, Republic of Korea

Corresponding author:*

Jung Hyun Kim: jhkim2011@hanbat.ac.kr, jhkim1870@gmail.com, Tel: +82-42-821-1239, Fax: +82-42-821-1592, Department of Advanced Materials Science and Engineering, Hanbat National University, 125, Dongseo-Daero, Yuseong-Gu, Daejeon, 34158, Republic of Korea

Abstract

The microstructural and electrochemical properties of anodes obtained by impregnation of the $La_{0.4}Sr_{0.6}Ti_{0.8}Mn_{0.2}O_{3\pm d}$ (LSTM) oxide system into two types of anode substrates such as Ni / 8YSZ substrate (Ni (E) / 8YSZ) and partially Ni removed Ni / 8YSZ substrate (Ni(R)/8YSZ) were investigated in order to apply them as anode material for solid oxide fuel cells.

All of the samples with LSTM impregnated on Ni (R) / 8YSZ show higher electrical conductivity values than those of unimpregnated Ni (E) / 8YSZ under dry H_2 condition. The highest electrical conductivity values of 2041.2, 1877.4, and 1764.3 S/cm at 700, 800 and 900 ^oC can be achieved by samples with 3 wt% impregnated LSTM on Ni (R) / 8YSZ. From the XPS analysis, the existence of a Ti metal peak on the surface of LSTM was only measured for the LSTM (3wt%)-Ni (R) / 8YSZ sample, metallic titanium on the surface can improve the electrical catalytic reaction.

LSTM (3wt%)-Ni (R) / 8YSZ showed higher electrical conductivity values then those of LSTM (3wt%)-Ni (E) / 8YSZ in all the temperature ranges measured in the case of dry CH_4 supply. Finally, the electrical conductivity of LSTM (3wt%)-Ni (R) / 8YSZ was stably maintained even when exposed to dry CH_4 condition at 900 ^oC for a long time (100 hours).

Keywords: Solid oxide fuel cell; Anode; Ni removed anode; Electrical conductivity; Impregnation

1. Introduction

Currently, the most commonly used anode material for Solid Oxide Fuel Cell (SOFC) operation is a cermet typed anode consisting of nickel oxide (NiO) and 8mol% yttria-stabilized zirconia (8YSZ), because Ni metal generated from the reduced NiO not only improves the catalytic performance at the SOFC anode, but also becomes the electron passage. 8YSZ prevents Ni coarsening that may occur during operation of the SOFC as well as also acts as an oxygen ion channel to expand the three-phase boundary (TPB) [1-6]. The material features of this cermet show excellent electrochemical properties and performance when using pure hydrogen fuel.

However, when hydrocarbon-based fuels are supplied to the SOFC anode composed of NiO / 8YSZ, carbon deposition on the surface and inside of the anode occurs which results in performance degradation and durability problems [1, 7, 8]. Therefore, in order to develop SOFC anode materials with excellent electrochemical properties and durability characteristics without carbon deposition, new anode materials with enhanced electrochemical properties and resistance to carbon formation have to be developed [9-13].

For the new anode materials, we proposed the concept of space formation technology and space replacement technology in anode materials for hydrocarbon driven SOFCs.

The space formation technology can be understood as additionally generated porous structures by partially removing Ni metal from Ni / 8YSZ anodes, the removal carried out by nitrate acid. The space replacement technology is to impregnate nitrate solutions into the porous anode structure and to generate single phase of perovskites in situ after the decomposition of the nitrates. In detail, these concepts combine the modification of the Ni-YSZ cermet by altering the nickel content carrying out surface treatment with adding oxide material catalysts and the synthesis of new single phase anode materials. In a related research study, we recently synthesized a $La_{0.4}Sr_{0.6}Ti_{0.8}Mn_{0.2}O_{3\pm d}$ (LSTM) oxide system on a porous 8YSZ scaffold structure using an impregnation technique, this fabrication representing space replacement technology [14] and subsequently analyzed its electrochemical properties.

In this study, we investigated the microstructural and electrochemical properties of a porous structure suitable for application as a SOFC anode fabricated by applying the concept of the space formation technology to a Ni / 8YSZ anode as well as the concept of the space replacement technology using LSTM.

2. Experimental

2.1. Fabrication of the NiO / 8YSZ substrate

NiO powder (J.T. Baker, USA) and 8 mol% yttria stabilized zirconia (8YSZ, Tosho, Japan) powder were mixed at a weight ratio of 6:4 for the fabrication of the NiO / 8YSZ substrate. In addition, 15 wt% of carbon black (J.T. Baker, USA) used as the pore former and 1wt% of Butvar B-98 (Sigma) used as binder were added to the mixture of NiO / 8YSZ.

The mixture for the fabrication of the substrate was ball-milled for 24 hours using ethanol as suspension medium. The powders were dried in the oven, pulverized using an agate mortar and sieved through a 100 micro sized mesh. The mixed powders were pressed into pellets of the shapes of rectangular prisms and then sintered at 1450 ^{o}C for 2 hours with a heating rate of 3 ^{o}C / min. After the sintering related shrinkage these pellet bars showed a compact size of 5.5 mm x 4 mm x 24 mm and were subsequently used for XPS, SEM, EDS and conductivity measurements.

2.2. Selective Ni-removal from the NiO / 8YSZ substrate

As the space formation technology for the partial removal of Ni from the NiO / 8YSZ

substrate, the NiO / 8YSZ substrate firstly was reduced to Ni / 8YSZ because Ni metal can be easily removed from the reduced substrate using a HNO_3 based solution. This Ni removal can result in an increase in the porosity of the substrate beyond the porous structure that existed previously caused by the pore former.

Table 1. Summary of abbreviations for samples used in this experiment.

Initial of samples	**Chemical composition or experimental condition**
LSTM	$La_{0.4}Sr_{0.6}Ti_{0.8}Mn_{0.2}O_{3\pm d}$
Ni (E) / 8YSZ	Reduced Ni / 8YSZ substrate
Ni (R) / 8YSZ	Partially Ni removed Ni / 8YSZ substrate, also reduced
LSTM (3wt%) -Ni (E) / 8YSZ	3 wt% impregnated LSTM onto the Ni (E) / 8YSZ substrate; then, heat treatment under reducing atmosphere
LSTM (3wt%) -Ni (R) / 8YSZ	3 wt% impregnated LSTM onto the partially Ni removed Ni / 8YSZ substrate [Ni (R) / 8YSZ]; then, heat treatment under reducing atmosphere

For this reason, fabricated NiO / 8YSZ substrates were exposed to reducing conditions by supplying 3.9 % H_2 / Ar balance gas at 930 ^oC for 20 hours in order to reduce the

NiO in the substrate to Ni. The reduced Ni / 8YSZ substrates obtained in this way were initialized as Ni (E) / 8YSZ, generally abbreviations used throughout this paper are displayed in Table 1.

These Ni (E) / 8YSZ substrates were dipped into an acid based solution consisting of a 1:1 volume ratio of HNO_3-H_2O. After the dipping process into the HNO_3-H_2O solutions, these substrates were washed with deionized water and then the remaining HNO_3 was removed by thorough washing with deionized water. After the washing process of the Ni (E) / 8YSZ substrates, they were dried in an oven at 80 ^oC. Partially Ni removed Ni / 8YSZ substrates obtained after this procedure were named Ni (R) / 8YSZ, generally abbreviations used throughout this paper are displayed in Table 1.

2.3. Impregnation process, prepared samples and XPS analysis

The space replacement technology aims to impregnate the Ni (E) / 8YSZ substrate and the selectively Ni removed porous structure Ni (R) / 8YSZ with a solution of nitrates, which will finally generate $La_{0.4}Sr_{0.6}Ti_{0.8}Mn_{0.2}O_{3\pm d}$ (LSTM). Lanthanum nitrate ($La(NO_3)_3$-$6H_2O$), Strontium nitrate ($Sr(NO_3)_2$), Dihydroxy-bis (ammonium lactato)-titanium (IV) ($[CH_3CH(O^-)CO_2$-$NH_4]_2$-$Ti(OH)_2$), Manganese nitrate ($Mn(NO_3)_2$-$4H_2O$) were weighed and mixed in deionized water forming a solution with a concentration as

low as 0.25 mol/L. In addition, the mixtures of raw materials were dissolved in distilled water without addition of glycine; this was done in order to prevent swelling problems caused by the repeated impregnation process.

Using a syringe, the solutions were slowly dropped onto the surface of the two porous substrates Ni (E) / 8YSZ and Ni (R) / 8YSZ. When the pores of the substrates became saturated with solution, the samples were heated to 500 ^{o}C in air to evaporate the solvent and to decompose the nitrates in the solution. This process was repeated many times until the desired weight of LSTM precursor was reached on the Ni (E) / 8YSZ and on the Ni (R) / 8YSZ substrates. The samples were calcined at 1200 ^{o}C for 4 hours in air to form a single phase of LSTM and then a final heat-treatment was carried out at 930 ^{o}C for 10 hours in order to create a uniform cover of LSTM over the Ni (E) / 8YSZ and over the Ni (R) / 8YSZ substrates. This uniform LSTM cover showing in oxidizing atmosphere transforms its appearance to fine particles when reduced.

The abbreviations used for the samples for XPS analysis are also summarized in Table 1. The abbreviation LSTM (3wt%)- Ni (E) / 8YSZ indicates that 3 wt% of LSTM was impregnated into the Ni (E) / 8YSZ substrate and then heat treated under reducing atmosphere. Finally, LSTM (3wt%)-Ni (R) / 8YSZ is 3 wt% of LSTM was impregnated onto partially Ni-removed Ni / 8YSZ substrate (Ni (R) / 8YSZ) and then heat treated

under reducing atmosphere. For the XPS analysis, a VG-Scientific ESCALAB 250 spectrometer (UK) with a monochromatic X-ray source was used. Detailed experimental procedures for XPS analysis can be found elsewhere [15-18].

2.4. Electrical conductivity measurement and microstructural characterization

Electrical conductivity measurements were conducted using a four-terminal DC arrangement in a custom jig with a Keithley 2400 Source Meter over a temperature range from 50 °C to 900 °C at a rate of 5 ^{o}C/min in a dry H_2 (3.9 % H_2 / Ar balance gas), wet H_2 and dry CH_4. The microstructural characteristics of the samples were investigated using field emission scanning electron microscopy (FE-SEM, S-4300, Hitachi) combined with energy dispersive spectroscopy (EDS).

3. Result and discussion

3.1. Weight loss of Ni from Ni/8YSZ substrate

Fig. 1 shows the weight loss behavior when reduced bar type Ni (E) / 8YSZ substrates were dipped into a HNO_3 based acid solution. When these samples were dipped into acid solution, abrupt weight losses with a ratio 3.32 wt.% / min. were

observed from the initial stage of contacting the solution to 5 minutes of measuring time, indicating that some of the Ni originating from reduction of NiO from the surface of Ni (E) / 8YSZ was dissolved into solution. This phenomenon can be related with equation (1)

$$Ni\,(s) + 4HNO_3\,(aq) \rightarrow Ni(NO_3)_2\,(aq) + 2H_2O\,(l) + 2NO_2\,(g) \quad \text{.....(1)}$$

After 5 minutes the slope of the weight loss ratio suddenly decreased to a much lower level, the gradient of the slope between 5 minutes and 120 minutes indicates an average weight loss of 2.29 x 10^{-2} wt%/min, this new reduced weight loss can also be ascribed to dissolution of Ni, but this time inside the Ni (E) / 8YSZ bars.

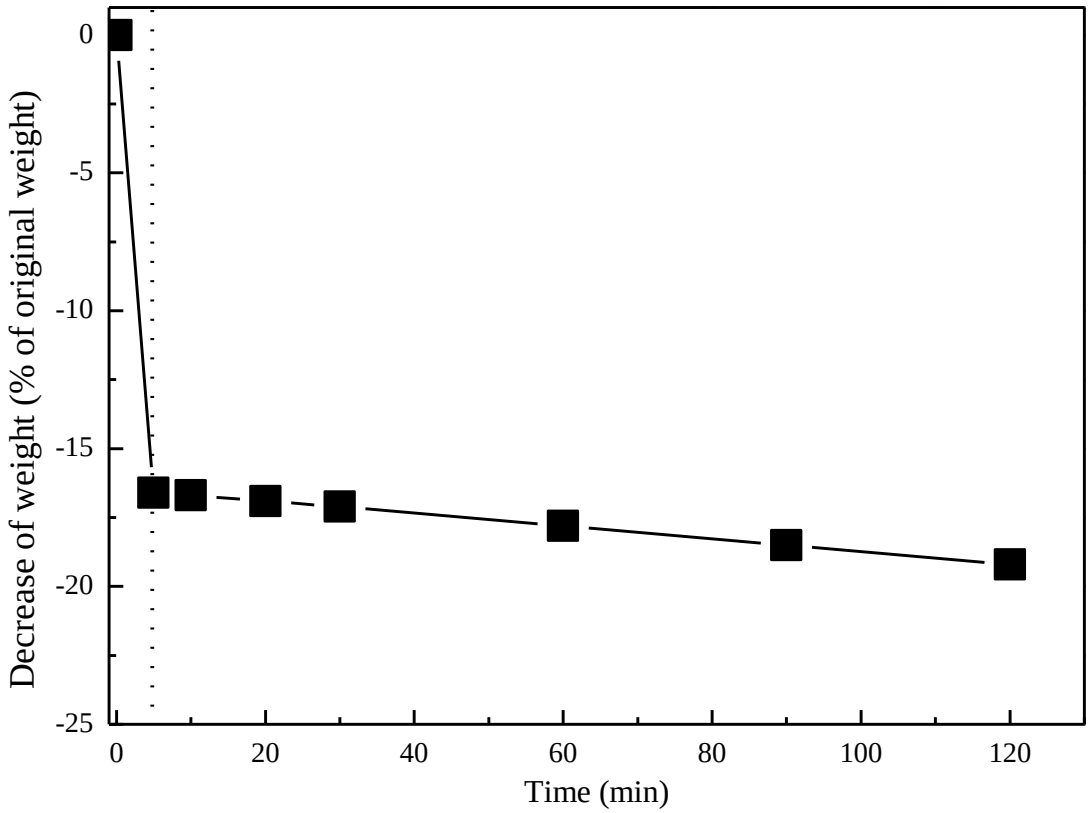

Fig. 1. Weight change characteristics of Ni (R) / 8YSZ substrates related to time of exposure to acid solution.

Therefore, the weight losses in the first stage of time (0~5 minutes) are ascribed to the dissolution of Ni located at the surface of reduced Ni (E) / 8YSZ and the weight losses in the second stage (5~120 minutes) originate from eluted Ni from the inside of reduced Ni (E) / 8YSZ.

From this result shown in Fig. 1 the optimization of the process time for surface Ni removal from Ni (E) / 8YSZ results in selective 5 minutes dipping in diluted nitric acid.

3.2. Microstructure of $La_{0.4}Sr_{0.6}Ti_{0.8}Mn_{0.2}O_{3\pm d}$ (LSTM) on a Ni / 8YSZ substrate : Ni (E) / 8YSZ

Fig. 2 summarizes the microstructures of the surface and cross section images of Ni (E) / 8YSZ impregnated with $La_{0.4}Sr_{0.6}Ti_{0.8}Mn_{0.2}O_{3\pm d}$ (LSTM) without Ni removal. The pictures in Fig. 2 are vertically ordered according to increasing weight ratio of impregnated LSTM, with the number of wt% displayed inside the pictures indicating the weight ratio of impregnated LSTM to the weight of the substrate. When the surface and the cross section images of impregnated LSTM on Ni (E) / 8YSZ substrates in Fig. 2 are compared, it seems that the impregnated LSTM shows in the form of small spherical particles, which are connected to each other, on top of the Ni (E) / 8YSZ substrate up to 5 wt% LSTM. From the microstructure of Fig. 2 (b), (d) and (f), it was possible to identify LSTMs formed with small particles on the Ni (E) / 8YSZ substrate.

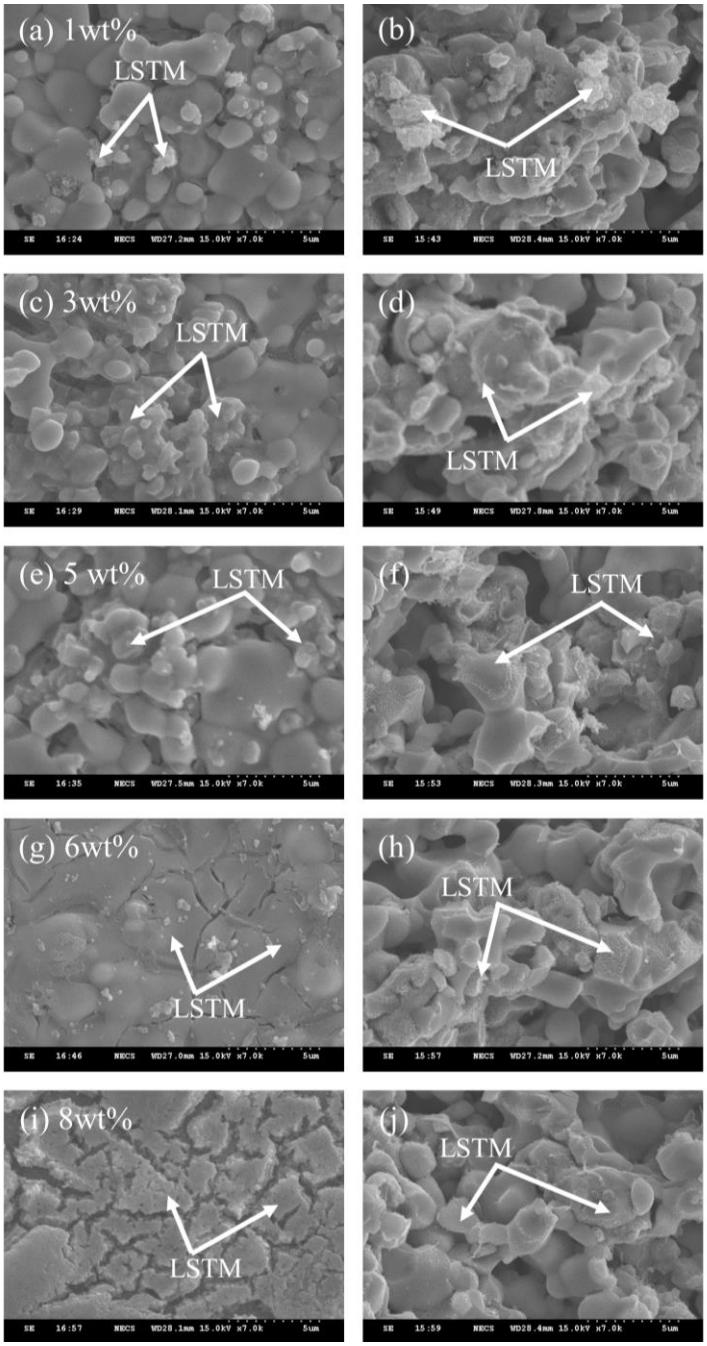

Fig. 2. SEM images of impregnated LSTM on Ni (E) / 8YSZ substrates. (a), (c), (e), (g) and (i) are top view images of the 1, 3, 5, 6 and 8 wt % impregnated LSTM on Ni (E) / 8YSZ substrates. (b), (d), (f), (h) and (j) are cross sample images of 1, 3, 5, 6 and 8 wt % impregnated LSTM on Ni (E) / 8YSZ substrates.

However, the microstructure covering the surface shows a large change when LSTM

is impregnated to an extent of more than 6 wt%, as shown in Fig. 2 (g). For example, as can be seen in Fig. 2 (g), the entire surface of Ni (E) / 8YSZ is covered with LSTM at 6wt% and the coagulation phenomenon and surface cracking of the impregnated LSTM are found at an impregnation level of 8 wt% LSTM, as depicted in Fig. 2 (i). In the images of sample cross sections similar microstructures can be observed over the whole range of impregnated percentage of LSTM. Samples with 6 wt% LSTM and more, as observed in Fig. 2 (h) and (j) show the same amount and distribution of LSTM particles as samples with 1, 3 and 5 wt% as observed in Fig. 2 (b), (d) and (f). As a result of the images of LSTM impregnated into Ni (E) / 8YSZ without Ni removal, it can be concluded that the microstructure of the surface was largely changed upon an impregnation level of more than 5% LSTM, while no large change between 5%, 6% and even 8% impregnated LSTM occurred in the areas further away from the surface as seen in the cross section. LSTM applied via impregnation in excess of 5 wt% apparently fails to intrude into the bulk of the Ni (E) / 8YSZ sample and instead builds up an LSTM layer on top of the surface on which the impregnation takes place. This top layer is increasing in thickness with increase of impregnated LSTM amount from 5 wt% to 6 wt% and 8 wt% eventually showing phenomena like coagulation and surface cracking.

3.3. Microstructure of LSTM on the partially Ni removed Ni / 8YSZ substrate: Ni (R) / 8YSZ

Fig. 3 displays the microstructural characteristics of impregnated LSTM on Ni (R) / 8YSZ substrates after Ni was partially removed from the surface of substrate. Comparing the results of Fig. 3 to Fig. 2, a significant change can be seen depending on the wt% of impregnated LSTM on the substrates. For example, the surface of Ni (R) / 8YSZ was uniformly coated with LSTM when 1 wt% of LSTM was impregnated, as can been seen in Fig. 3. (a).

The surface microstructure that can be observed at 3wt% shows that the impregnated LSTM was uniformly distributed on the grains and grain boundaries of 8 mol% yttria stabilized zirconia (8YSZ), the LSTM particles at the YSZ grain boundaries were at least partly connected to each other, while the LSTM particles located on top of YSZ grains were singular spheres with a slightly smaller diameter compared to the particles at the grain boundary.

Increasing the weight ratio of LSTM to 5 wt%, as shown in Fig. 3 (e), it can be seen that the impregnated LSTM was uniformly coating the substrate and the thickness of the impregnated LSTM layer was confirmed to be increased when comparing to Fig. 3 (a) and (b). In case of 6wt% impregnated LSTM, as shown in Fig. 3 (g), a large amount of

LSTM was impregnated on the surface of the grains and at an impregnation level of 8 wt% LSTM, additional LSTM particles were mainly grown to cover the gain boundaries of 8YSZ as displayed in Fig. 3 (i). When it comes to the microstructure of impregnated LSTM from the cross section images, no obvious differences in interface were found.

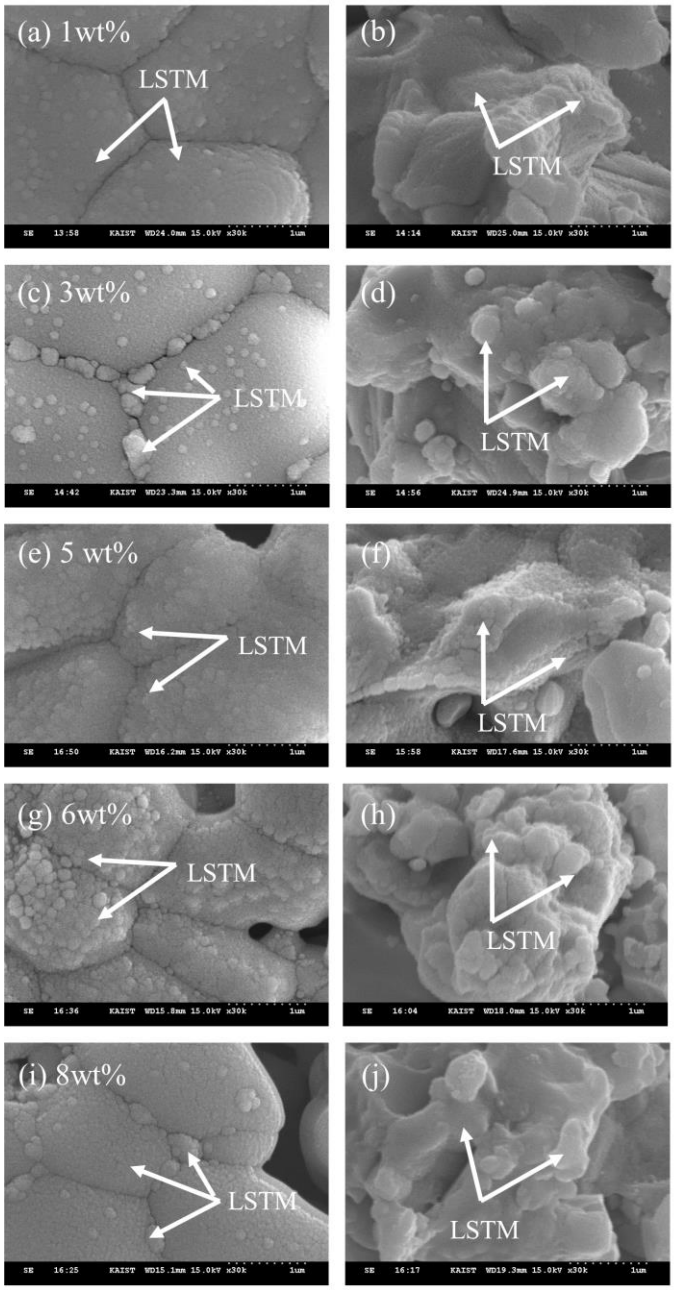

Fig. 3. SEM images of impregnated LSTM on Ni (R) / 8YSZ substrates. (a), (c), (e), (g) and (i) are top view images of the 1, 3, 5, 6 and 8 wt % impregnated LSTM on Ni (R) / 8YSZ substrates. (b), (d), (f), (h) and (j) are cross images of 1, 3, 5, 6 and 8 wt % impregnated LSTM on Ni (R) / 8YSZ substrates. The samples in this paper were sintered at 1200 ^{o}C for 1 hour under reducing condition.

In summary pictures of LSTM impregnated onto a Ni (R) / 8YSZ substrate showed that with increased contents of impregnated LSTM, additional LSTM particles showed on top of YSZ grains first, and at the grain boundaries of the substrate at a later stage. Growth of LSTM on grain boundaries with increased wt% of impregnation were repeatedly progressed from the surface of impregnated LSTM on Ni (R) / 8YSZ substrates. Furthermore the cross section images of Ni (R) / 8YSZ samples show a clear progression of the amount of visible LSTM particles from low LSTM content in Fig. 3 (b) and (d) over medium LSTM content in Fig. 3 (f) to high LSTM content in Fig. 3 (h) and (j). From this it is obvious that the intrusion of LSTM away from the impregnated surface into the bulk of Ni (R) / 8YSZ worked much better than into the bulk of Ni (E) / 8YSZ, probably because the passage of LSTM through Ni (R) / 8YSZ is easier because of its enhanced porosity.

Therefore, it can be concluded that the microstructure of impregnated LSTM was dependent on the substrate. In other words, in case of Ni (E) / 8YSZ pellets without Ni removal, the impregnated LSTM was just coated on the surface of a relatively dense support, the exact location of the growth of LSTM could not be determined and the question if it grows predominantly on grains or on grain boundaries at a certain level of impregnation, could not be answered.

However, when LSTM was coated on the relatively porous structure of Ni removed Ni (R) / 8YSZ bars using the impregnation technique, the location of growth of LSTM on the grains and grain boundaries of the substrate was observed.

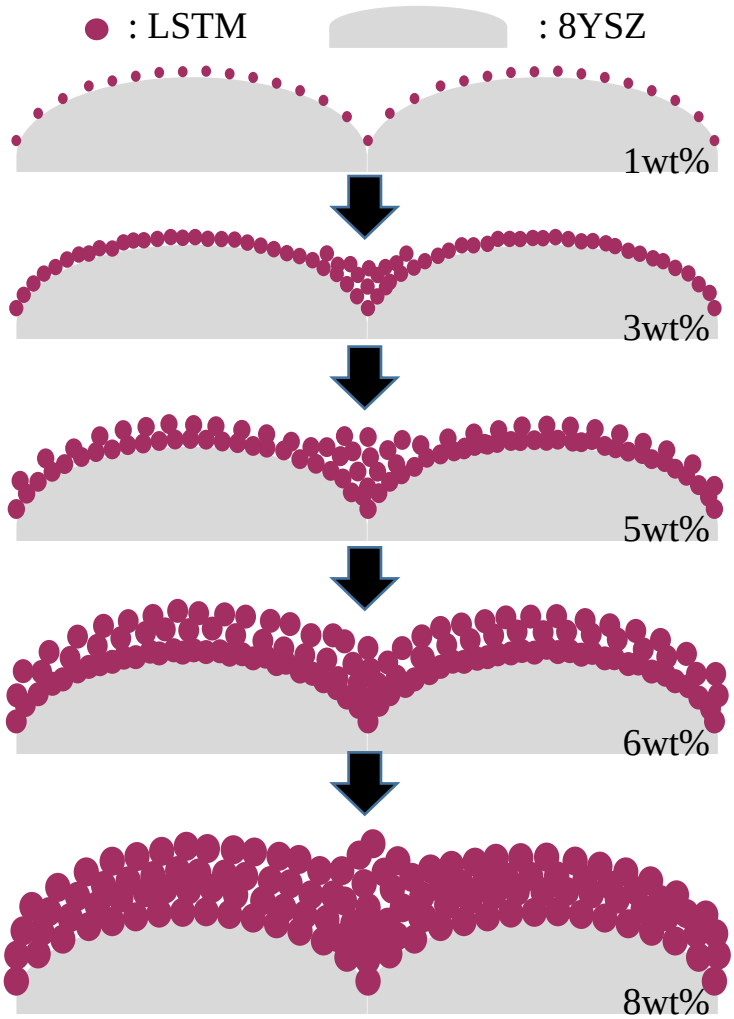

Fig. 4. Conceptual diagram showing the microstructure formation process of impregnated LSTM on Ni (R) / 8YSZ substrate

A conceptual diagram showing the microstructure formation process of impregnated LSTM on the Ni-free substrate is shown in Fig. 4.

Impregnated LSTM particles coat the surface of 8YSZ as singular spheres when the impregnation amount is 1 wt%, which is a relatively low concentration. When the impregnation amount is increased to 3 wt%, the size of the impregnated particles increases and the connectivity between the spherical particles is increased at the same time. Particularly in this case, LSTM particles are mainly grown at the grain boundaries. The level of 3 wt% LSTM impregnation produces samples with an optimized microstructural characteristic, providing maximal electron and ion mobility over a connected network of LSTM particles while effectively minimizing the impregnated amount of LSTM.

At more than 5 wt%, it can be seen that additional LSTM is deposited on the LSTM surface generated by impregnation on the surface of 8YSZ, creating particles of a larger diameter than the particles observed at 3 wt%. Thereafter, growth of both the layer thickness and the particle size of the LSTM continuously proceeds.

3.4. Electrical conductivity of LSTM on the Ni / 8YSZ substrate: Ni (E) / 8YSZ

Fig. 5 summarizes the electrical conductivities of LSTM impregnated samples of a Ni

(E) / 8YSZ substrate without Ni removal with respect to the dry and wet H_2 condition from 500 to 900 ^oC.

The number located behind "LSTM" means the number of impregnations of LSTM which have been conducted into the Ni (E) / 8YSZ substrate. As can be seen from Fig. 5 (a), the measured electrical conductivities of the Ni (E) / 8YSZ substrate without LSTM impregnation under dry H_2 condition were 663.6, 619.2, and 567.4 S/cm at 700, 800 and 900 ^oC. The electrical conductivities measured at one time impregnated LSTM-1 on Ni (E) / 8YSZ showed values of 100.8, 94.8, 88.5 S/cm at the same temperatures tested, which constitutes a significant decrease in conductivity compared to the pure Ni (E) / 8YSZ substrate conductivity. In fact, all of impregnated samples such as LSTM-1, 2, 3, 4 and 5 show lower electrical conductivity values than those of the Ni (E) / 8YSZ substrate and they display typically metallic conductivity behavior with respect to the temperature.

The relationship between conductivity and weight percentage of impregnated LSTM is summarized in Fig. 5 (b). When the increased weight and the number of impregnation were compared, it was confirmed that the impregnation of 1 time increased the weight by about 1 wt% compared to the Ni (E) / 8YSZ. In the case of 2 impregnation steps, a weight increase of 3wt% was confirmed. Three, four and five impregnation steps led to

5wt%, 6wt% and 8wt% impregnated LSTM respectively. From the results of Fig. 5 (b), it can be seen that in the range between 0wt% of LSTM and 3wt% of LSTM, the electrical conductivities decreased with increasing impregnated material, however, the values of electrical conductivity increased with increased contents of LSTM impregnated into the Ni (E) / 8YSZ substrate from 3 wt% upwards. These characteristics can be confirmed not only in dry hydrogen atmosphere shown in Fig. 5 (a) and (b) but also under wet H_2 conditions displayed in Fig. 5 (c) and (d).

Fig. 5 (e) displays the conductivity values of the different content LSTM samples impregnated into Ni (E) / 8YSZ, measured under dry and wet H_2 conditions. The electrical conductivities under dry and wet H_2 conditions showed almost the same values under dry and wet H_2 for samples from 1 wt % of LSTM-1 to 5wt% of LSTM-3. However, the conductivity values of 6 and 8wt % of LSTM-4 and 5 under wet H_2 conditions were relatively higher than the conductivity values measured under dry H_2 conditions.

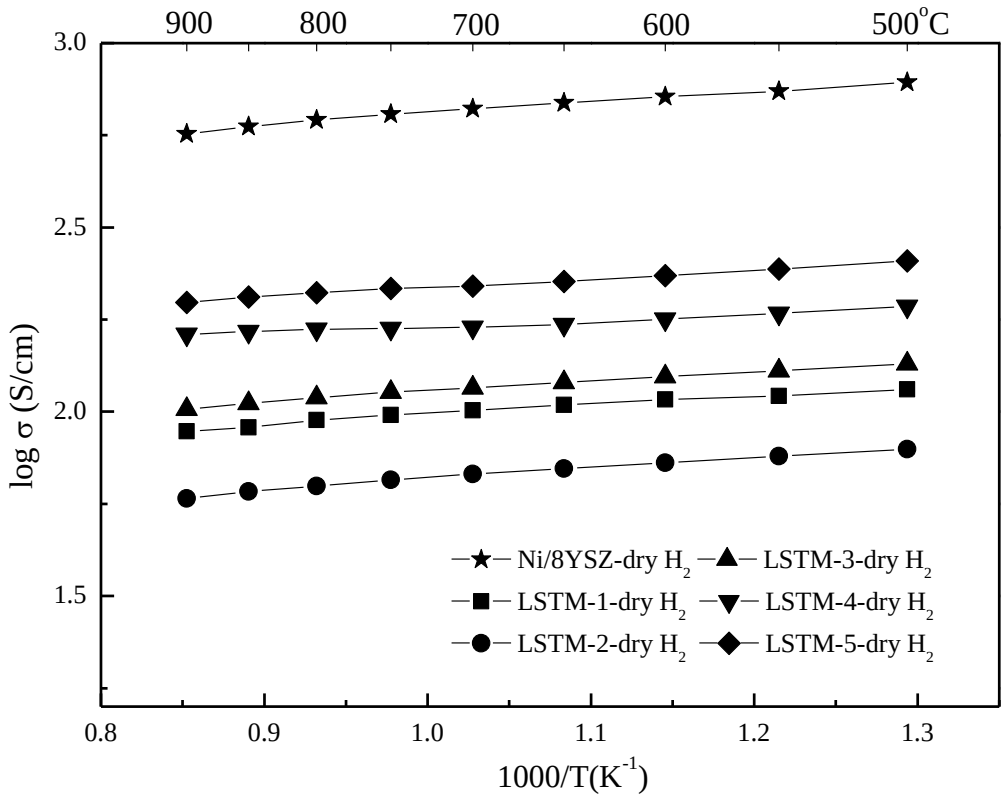
900
800
700
600
500°C
3.0
2.5
2.0
1.5
log σ (S/cm)
0.8
0.9
1.0
1.1
1.2
1.3
1000/T(K-1)
Ni/8YSZ-dry H2
LSTM-3-dry H2
LSTM-1-dry H2
LSTM-4-dry H2
LSTM-2-dry H2
LSTM-5-dry H2

Fig. 5. (a)

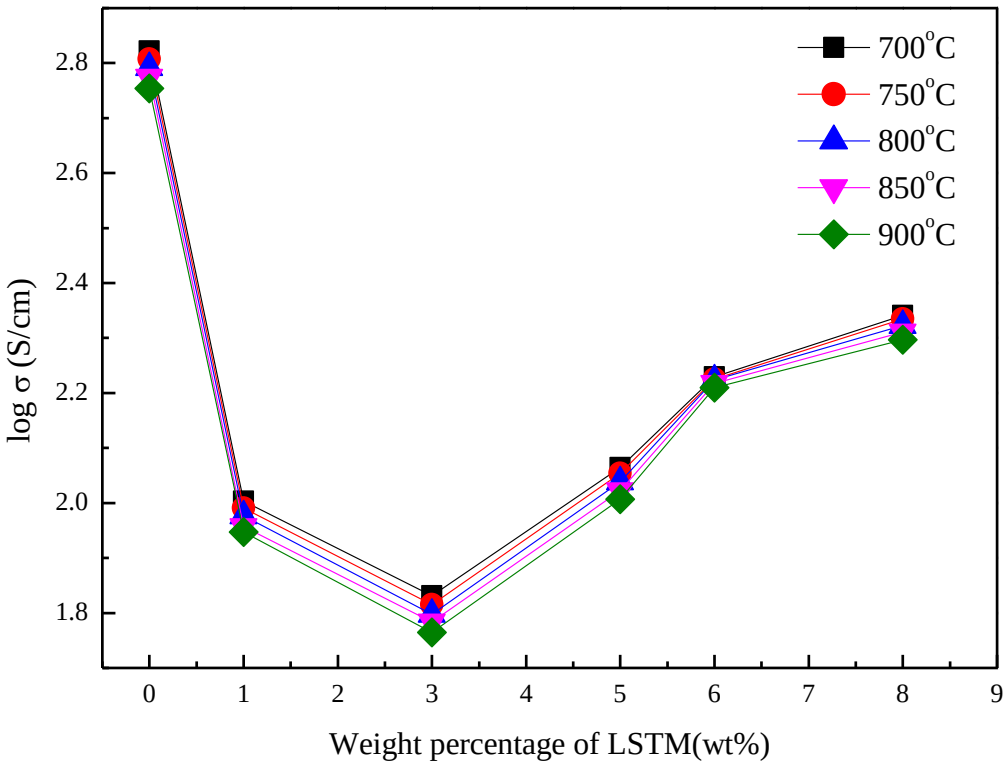
700°C
750°C
800°C
850°C
900°C
2.8
2.6
2.4
2.2
2.0
1.8
log σ (S/cm)
0
1
2
3
4
5
6
7
8
9
Weight percentage of LSTM(wt%)

Fig. 5. (b)

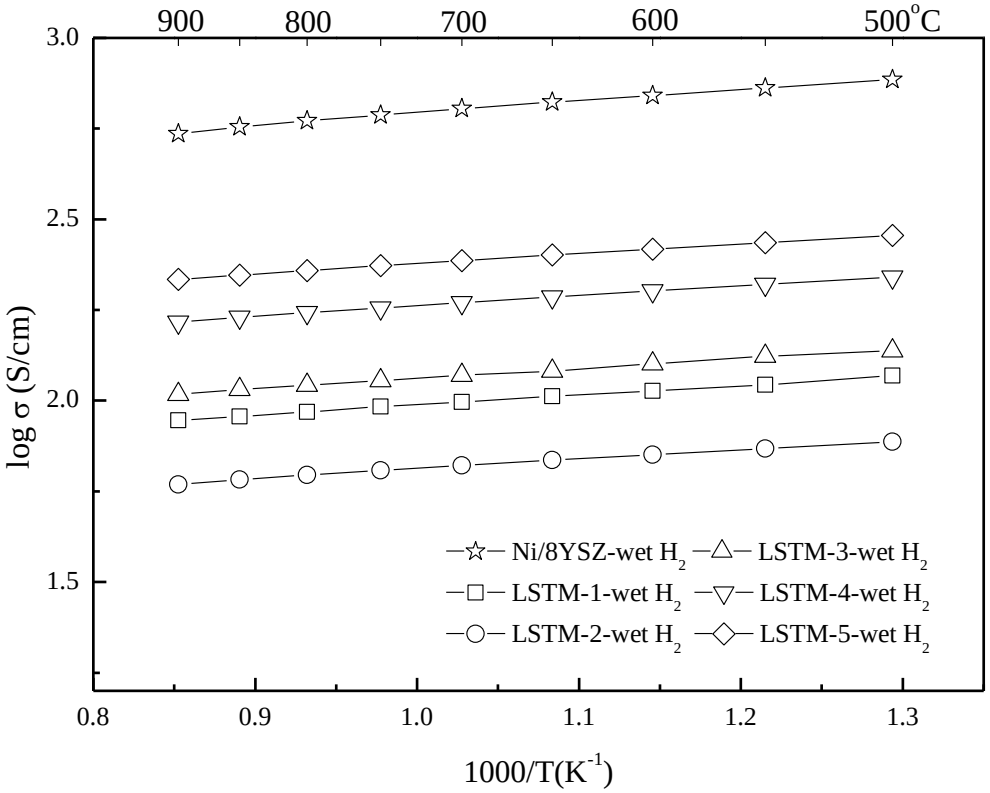
900
800
700
600
500°C
3.0
2.5
2.0
1.5
log σ (S/cm)
0.8
0.9
1.0
1.1
1.2
1.3
1000/T(K-1)
Ni/8YSZ-wet H2
LSTM-3-wet H2
LSTM-1-wet H2
LSTM-4-wet H2
LSTM-2-wet H2
LSTM-5-wet H2

Fig. 5. (c)

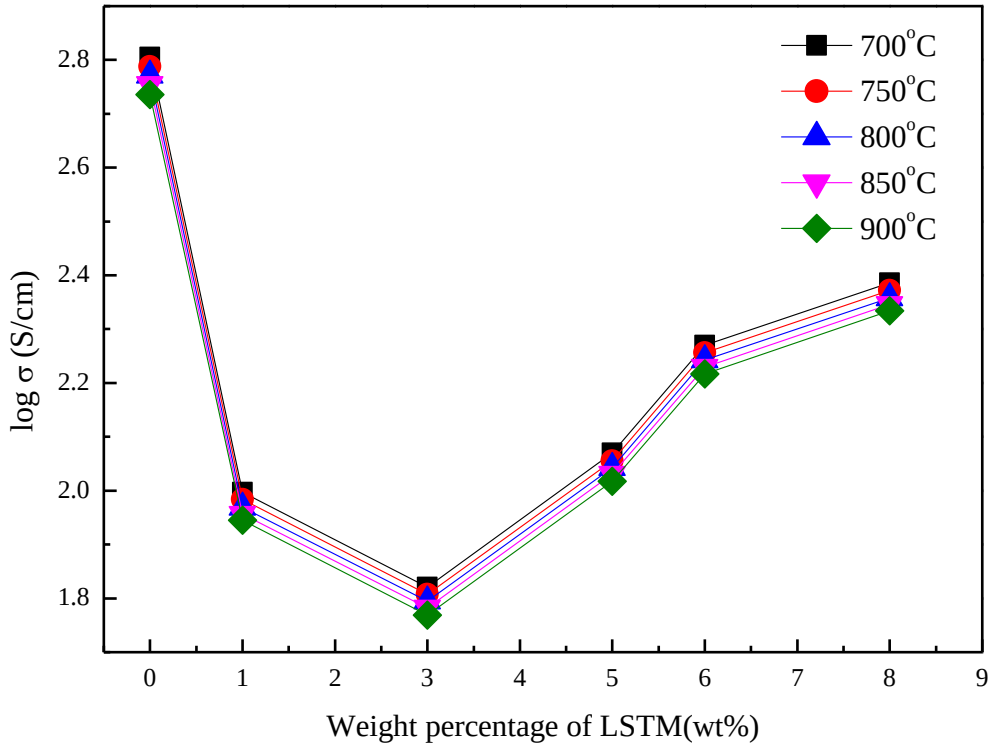
700°C
750°C
800°C
850°C
900°C
2.8
2.6
2.4
2.2
2.0
1.8
log σ (S/cm)
0
1
2
3
4
5
6
7
8
9
Weight percentage of LSTM(wt%)

Fig. 5. (d)

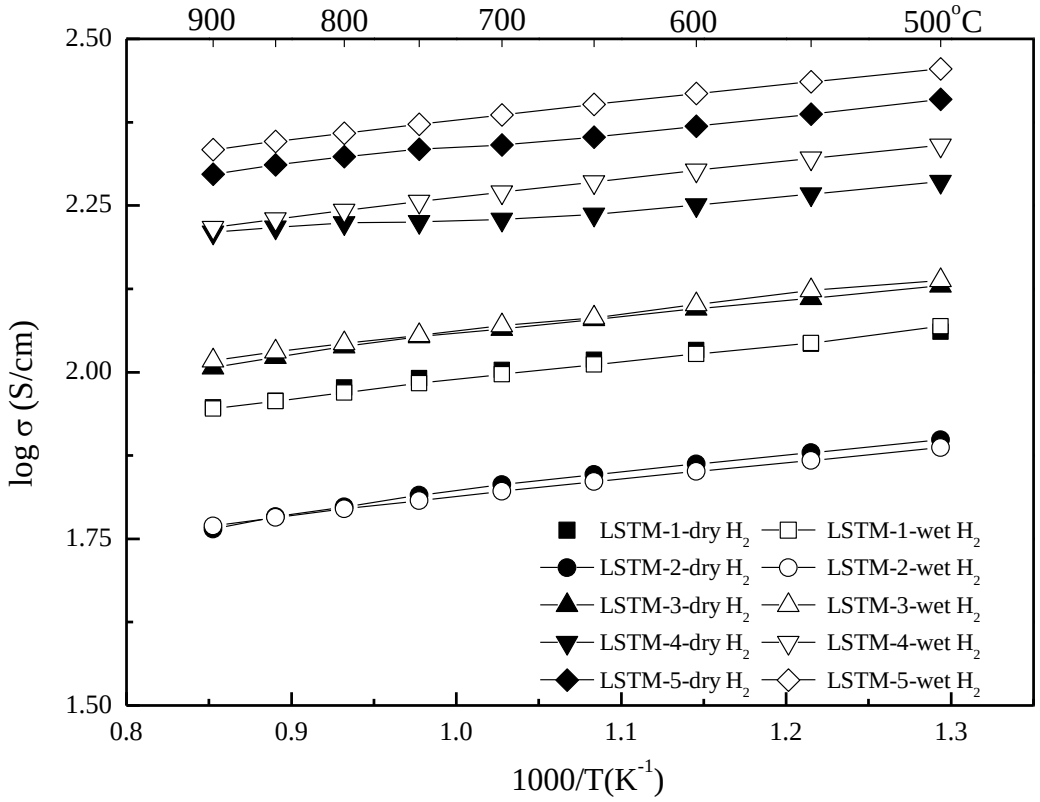

Fig. 5. (e)

Fig. 5. Summary of the electrical conductivities. (a) of LSTM impregnated Ni (E) / 8YSZ measured under dry H_2 condition from 500 to 900 °C. The number located behind LSTM means the number of performed LSTM impregnations into the substrate. (b) of LSTM impregnated Ni (E) / 8YSZ under dry condition with respect to the weight % of impregnated LSTM instead of the number of impregnation steps. (c) of LSTM impregnated Ni (E) / 8YSZ measured under wet H_2 condition from 500 to 900 °C. (d) of LSTM impregnated Ni (E) / 8YSZ under wet condition with respect to the weight % of impregnated LSTM instead of the number of impregnation steps. (e) summarized conductivity results measured under dry and wet H_2 conditions.

3.5. Electrical conductivity of LSTM on the Ni removed Ni / 8YSZ substrate: Ni (R) / 8YSZ

Fig. 6 (a) shows the electrical conductivity properties of LSTM impregnated samples of a selectively Ni removed Ni (R) / 8YSZ substrate, considering that this substrate has a relatively more porous structure than Ni (E) / 8YSZ. In case of the conductivity of LSTM samples onto Ni (R) / 8YSZ substrates under dry H_2 reducing conditions, the electrical conductivity values of samples impregnated with LSTM were surprisingly much higher than those of the pure Ni (E) / 8YSZ sample. For example, LSTM-1-dry shows the electrical conductivity values of 1519.6, 1402.0, 1336.6 S/cm at 700, 800 and 900 ^{o}C respectively. Compared with the results of the LSTM-1-dry sample impregnated into the Ni (E) / 8YSZ substrate (100.8, 94.8, 88.5 S/cm at the same temperature ranges measured), which were discussed before, these conductivity results are almost 10 times higher. Observing the conductivity tendency of impregnated LSTM into Ni free Ni (R) / 8YSZ substrate, it also shows the metallic behavior found in Ni (E) / 8YSZ. The magnitude of the electrical conductivity values observed in LSTM-1-dry on Ni (R) / 8YSZ is also much higher than that of the unimpregnated Ni (E) / 8YSZ. For LSTM-1, 2, 3, 4, and 5 samples, the LSTM-1 sample showed the lowest electrical conductivity and the LSTM-2 sample showed the highest electrical conductivity.

In addition to these results, the electrical conductivity characteristics with respect to temperature and composition are summarized in Fig. 6 (b). Conductivity values decreased with increasing temperature in all compositions. However, in the case of composition, various characteristics were found depending on the amount of LSTM impregnated in selectively Ni removed Ni (R) / 8YSZ substrates. For example, increasing contents of the LSTM from 0 wt% (Ni (E) / 8YSZ) to 3 wt% (LSTM-2) increased the electrical conductivity, and the highest electrical conductivity of all samples was found in the LSTM-2 sample (LSTM-2 indicates 3wt% of LSTM was impregnated into Ni (R) / 8YSZ substrate). The electrical conductivity values of LSTM-2 were 2041.2, 1877.4, and 1764.3 S/cm at 700, 800 and 900 ^{o}C. On the other hand, when the amount of LSTM impregnated into the Ni (R) / 8YSZ substrate exceeded 3 wt%, the electrical conductivity decreased. These characteristics are the same in wet reducing conditions, as shown in Fig. 6 (c) and (d).

Fig. 6 (e) shows the complete collection of electrical conductivity values at a temperature range of 500 °C to 900 °C under dry and wet reducing conditions. It can be seen that all conductivity values measured under the dry H_2 conditions are higher than those measured under the wet H_2 conditions.

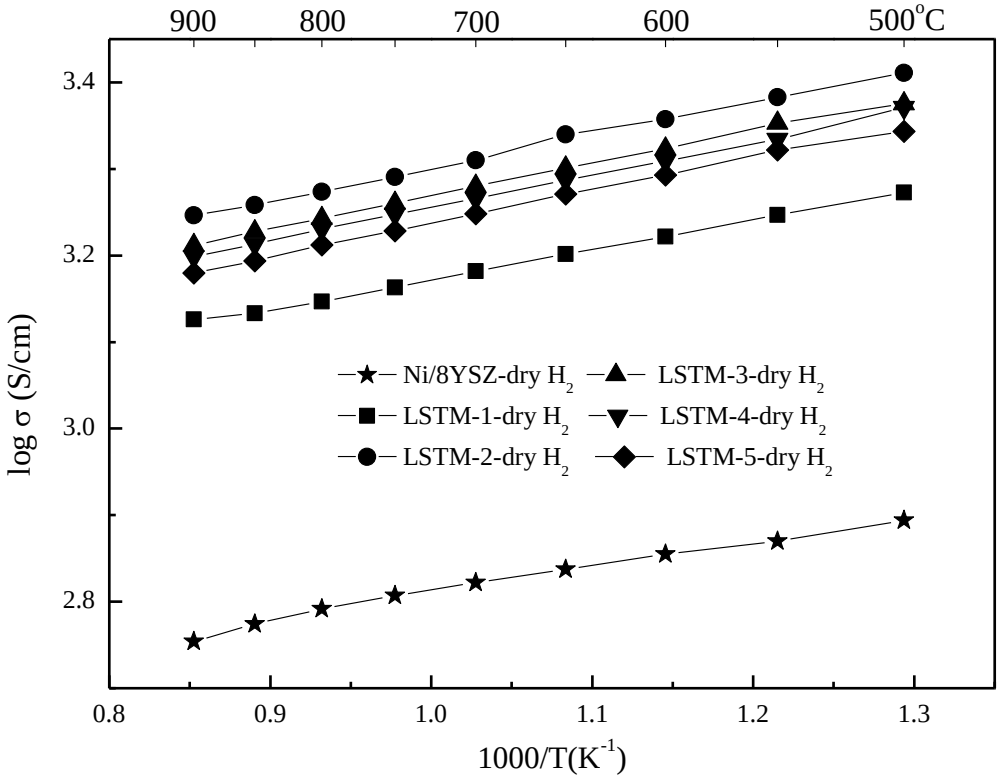
900
800
700
600
500°C
3.4
3.2
3.0
2.8
log σ (S/cm)
Ni/8YSZ-dry H2
LSTM-3-dry H2
LSTM-1-dry H2
LSTM-4-dry H2
LSTM-2-dry H2
LSTM-5-dry H2
0.8
0.9
1.0
1.1
1.2
1.3
1000/T(K-1)

Fig. 6. (a)

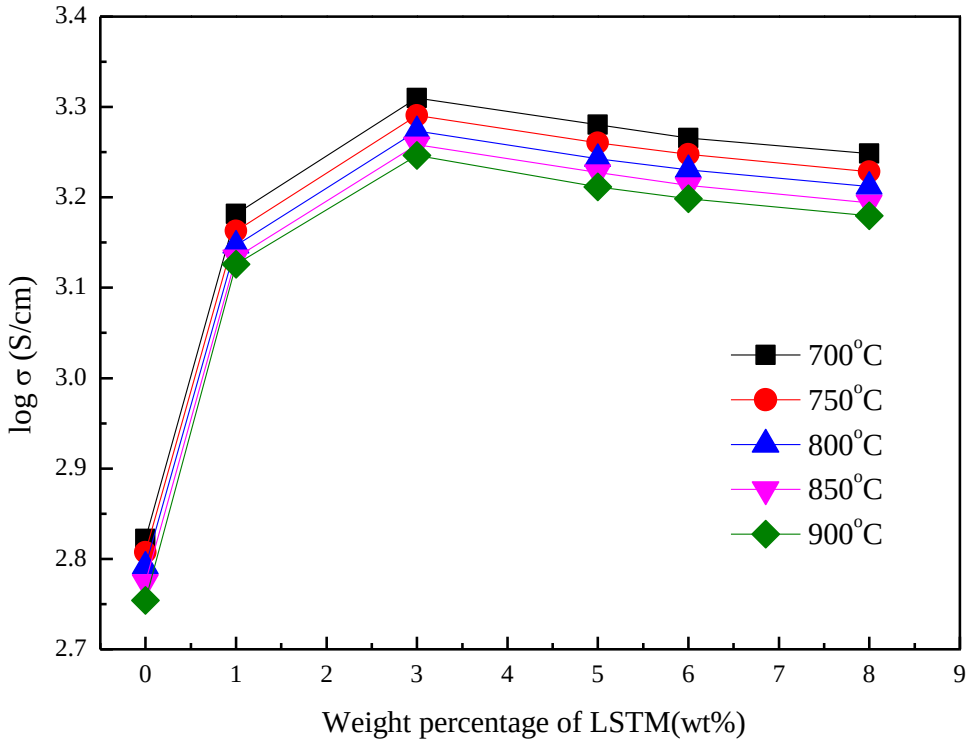
3.4
3.3
3.2
3.1
3.0
2.9
2.8
2.7
log σ (S/cm)
700°C
750°C
800°C
850°C
900°C
0
1
2
3
4
5
6
7
8
9
Weight percentage of LSTM(wt%)

Fig. 6. (b)

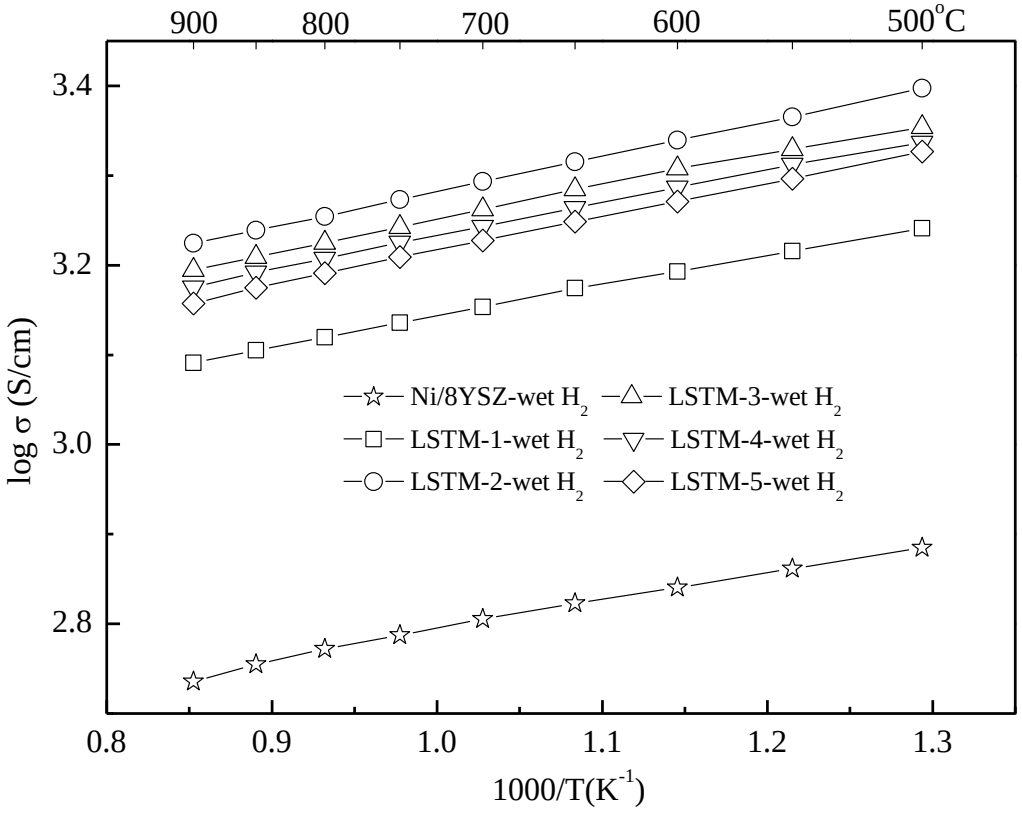
900
800
700
600
500°C
3.4
3.2
3.0
2.8
log σ (S/cm)
Ni/8YSZ-wet H2
LSTM-3-wet H2
LSTM-1-wet H2
LSTM-4-wet H2
LSTM-2-wet H2
LSTM-5-wet H2
0.8
0.9
1.0
1.1
1.2
1.3
1000/T(K-1)

Fig. 6. (c)

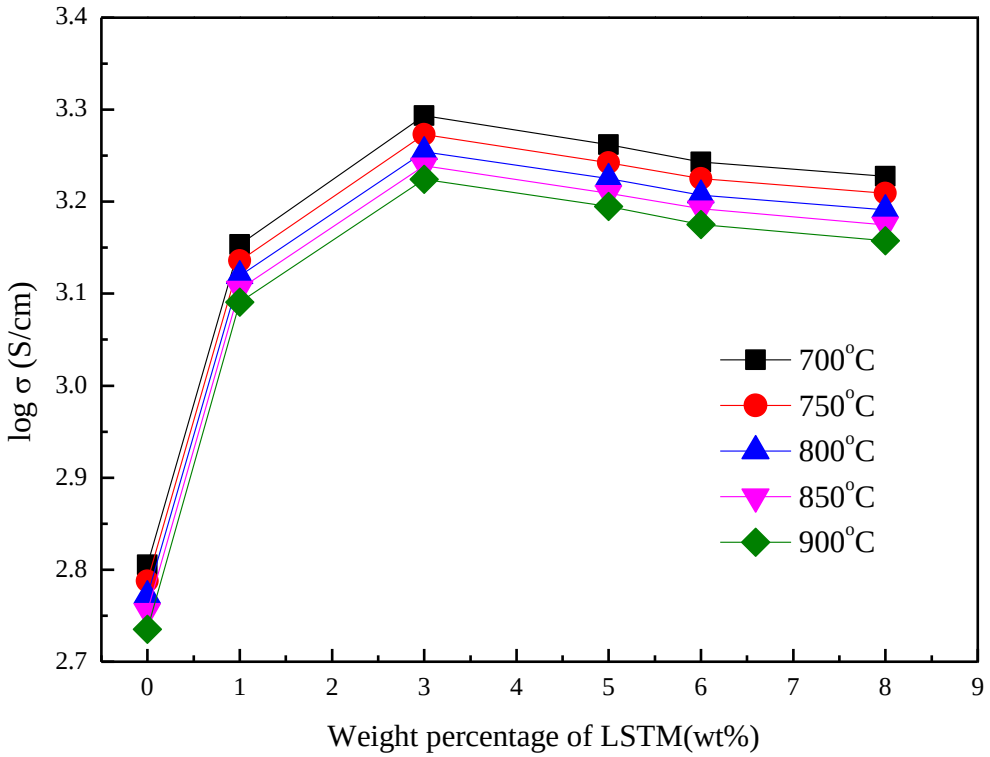
3.4
3.3
3.2
3.1
3.0
2.9
2.8
2.7
log σ (S/cm)
700°C
750°C
800°C
850°C
900°C
0
1
2
3
4
5
6
7
8
9
Weight percentage of LSTM(wt%)

Fig. 6. (d)

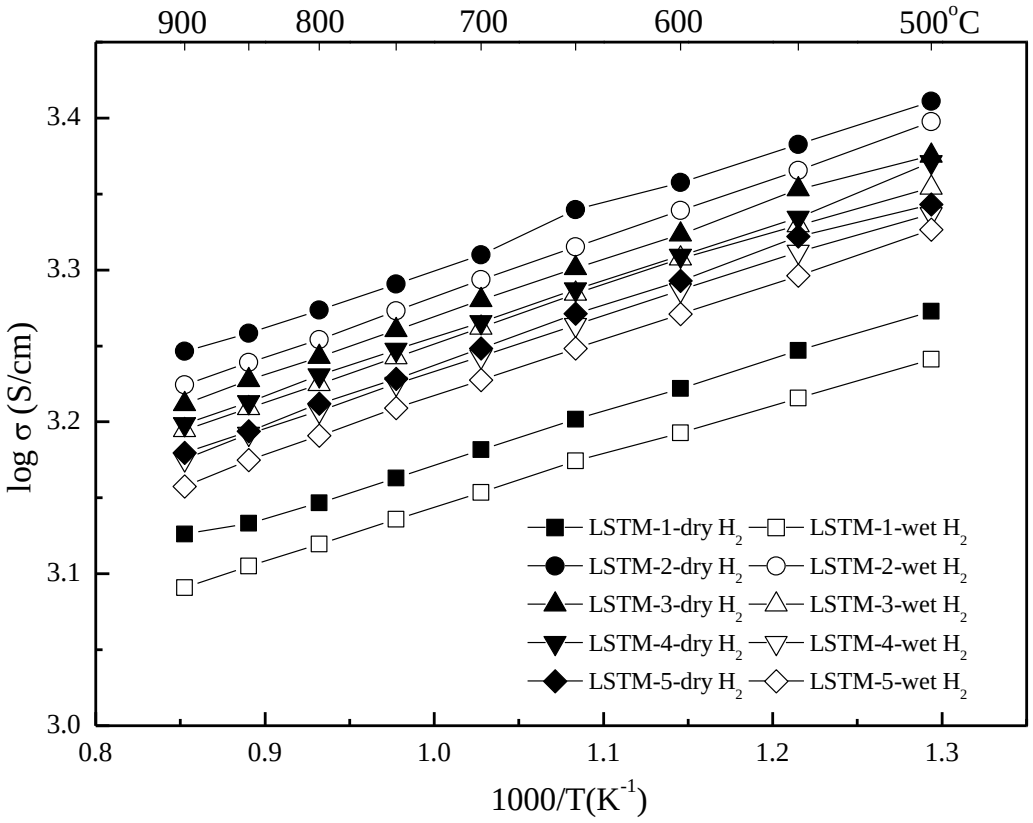

Fig. 6. (e)

Fig. 6. Summary of the electrical conductivities. (a) of LSTM impregnated Ni (R) / 8YSZ measured under dry H_2 condition from 500 to 900 °C. The number located behind LSTM means the number of performed LSTM impregnations into the substrate. (b) of LSTM impregnated Ni (R) / 8YSZ under dry condition with respect to the weight % of impregnated LSTM instead of the number of impregnation steps. (c) of LSTM impregnated Ni (R) / 8YSZ measured under wet H_2 condition from 500 to 900 °C. (d) of LSTM impregnated Ni (R) / 8YSZ under wet condition with respect to the weight % of impregnated LSTM instead of the number of impregnation steps. (e) summarized conductivity results measured under dry and wet H_2 conditions.

3.6. Energy dispersive spectrometer (EDS) analysis

As mentioned above, 3 wt% of impregnated LSTM on the Ni (R) / 8YSZ substrate showed the highest conductivity, which can be correlated with surface component analysis using Energy Dispersive Spectroscopy (EDS) analysis.

Fig. 7 and Table 2 summarize the results of the EDS analysis of Fig. 3 (c), obtained from a sample of 3 wt% LSTM on Ni (R) / 8YSZ annealed at 930 °C for 10 h in a reducing atmosphere. From these EDS results, location 'a' corresponds to the impregnated LSTM particles observed at the grain boundaries of 8YSZ comprised of Ni (R) / 8YSZ. In addition, location 'b' also indicates a bead-shaped point of the impregnated LSTM, located on a grain. The EDS results are summarized in Table 2.

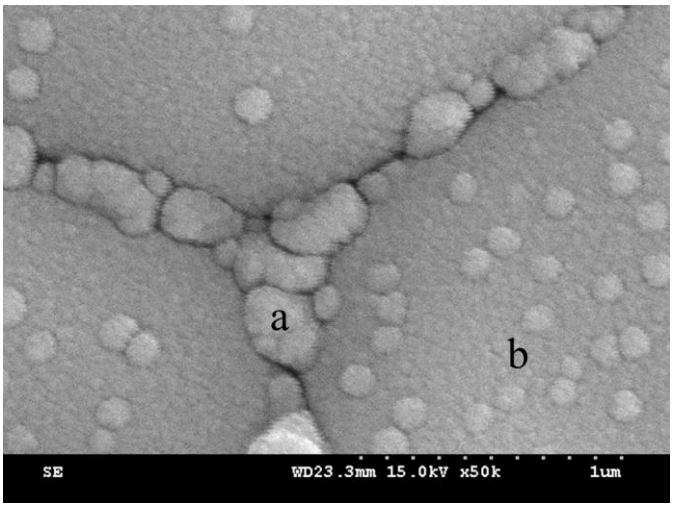

Fig. 7. Bright-field SEM image of the LSTM particles on Ni (R) / 8YSZ from an anode substrate exposed to humidified H_2 at 1200 ^oC. The letters indicate the locations where the EDS analysis was performed.

In Table 2, the highest concentration of Ti in LSTM was found at point ‘a’. On the other hand, location ‘b’ shows a much lower concentration of Ti. Therefore, it can be concluded that the higher conductivities of the sample with the impregnated LSTM on the Ni (R) / 8YSZ substrate are caused by the presence of Ti observed at the grain boundary. The result of this analysis can be also correlated with the Ti metal peaks using XPS investigation in the next part.

Table 2. Energy Dispersive Spectrometer (EDS) analysis results of different sample locations marked a and b in Fig. 7.

Element	**Atomic weight %**	
	a	**b**
Ni	15.92	11.80
Zr	73.86	87.39
La	3.65	0.81
Sr	3.04	-1.07
Ti	3.79	1.19
Mn	-0.26	-0.11
Totals	100	100

3.7. XPS spectra of Ti

The deconvolution results in Fig. 8 and the summarized results in Table 3 lead to the assumption that various charge states of Ti are present. The BEs of the types of Ti^{2+}, Ti^{3+} and Ti^{4+} are located in almost the same BE ranges; this agrees with our previous experiment on Ti containing complex perovskites [15], as well as with the literature [19-21]. For example, the XPS peak of TiO with a charge of Ti^{2+} is reported in literature at BEs of 455.5 eV (Ti $2p_{3/2}$) and 461.1 eV (Ti $2p_{1/2}$) and the XPS peak of Ti_2O_3 with a charge of Ti^{3+} is reported at 457.3 eV (Ti $2p_{3/2}$) and 462.5 eV (Ti $2p_{1/2}$). In addition, in literature the evidence for the presence of Ti^{4+} of the oxide type of TiO_2 is constituted by the observation of peaks at 458.7 eV (Ti $2p_{3/2}$) and 464.3 eV (Ti $2p_{1/2}$) [15, 19-21].

From Table 3, both LSTM (3wt%)-Ni (E) / 8YSZ and LSTM (3wt%)-Ni (R) / 8YSZ showed the largest part of the integrated area at peaks with a position related to Ti_2O_3, with the area % values of 41.79 and 68.02. Obviously the largest part of the available titanium ions occurs in the charge state of Ti^{3+} in both samples. In summary, a change of Ti to a lower charge valence state is observed in this XPS analysis under reducing conditions, for example the change of Ti^{4+} to Ti^{3+}, a valence change that is believed to be induced or promoted by the presence of LSTM. It can be said that the presence of various charge valences such as Ti^{4+} and Ti^{3+} can supply a path for improved electron

transport and provide additional pathways for redox reactions in the LSTM oxide system.

The ratio of Ti^{3+} / Ti^{4+} and the charge sate of Ti in different samples with various experimental history are also summarized in Table 3. The ratios of Ti^{3+} / Ti^{4+} from LSTM (3wt%)-Ni (E) / 8YSZ and LSTM (3wt%)-Ni (R) / 8YSZ were calculated and found to be 1.14 and 3.40. The calculated charge states of Ti can be expressed as 3.15 and 3.10, showing that the average charge of Ti in the samples decreased in the reducing process because a greater concentration of Ti^{3+} was present, instead of Ti^{4+}.

Significantly, in the case of the Ti satellite peak shown in Fig. 8 (b), LSTM (3wt%)-Ni (R) / 8YSZ is the only composition which shows evidence of this satellite peak under fully reduced conditions, when comparing it to the XPS spectrum of fully reduced LSTM (3wt%)-Ni (E) / 8YSZ (Fig. 8 (a)), the satellite peak could not be found there. The satellite peak was observed at around 460.5 eV and this BE value is very close to the value (460.6 eV) of Ti metal $2p_{1/2}$ reported by M. K. Rath's group [19]. In other words, the existence of a Ti metal peak on the surface of LSTM was exclusively measured at samples of fully reduced LSTM (3wt%)-Ni (R) /8YSZ ; the metallic titanium creating this peak can improve the electrical catalytic reaction.

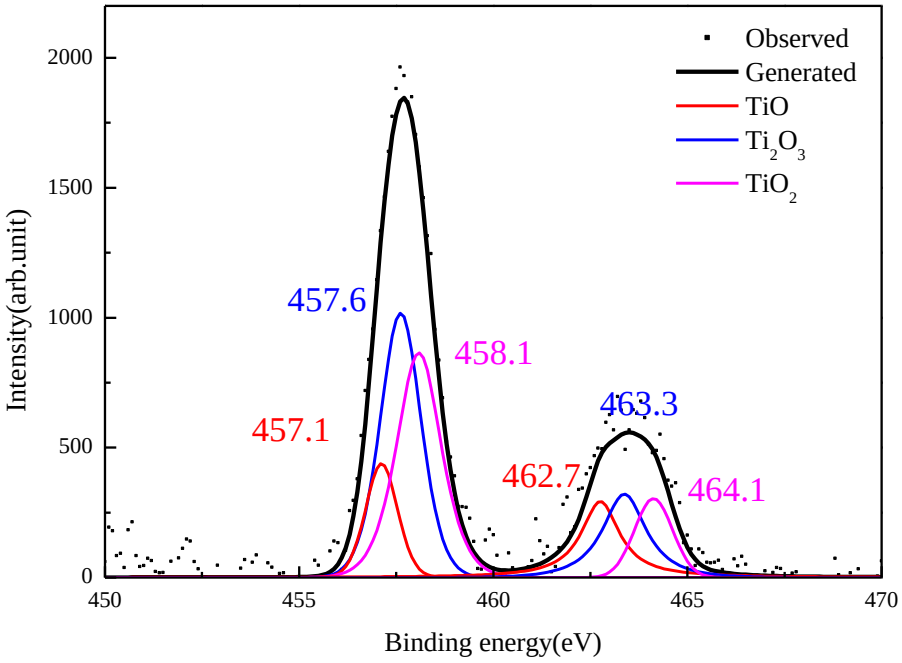

Fig. 8. (a)

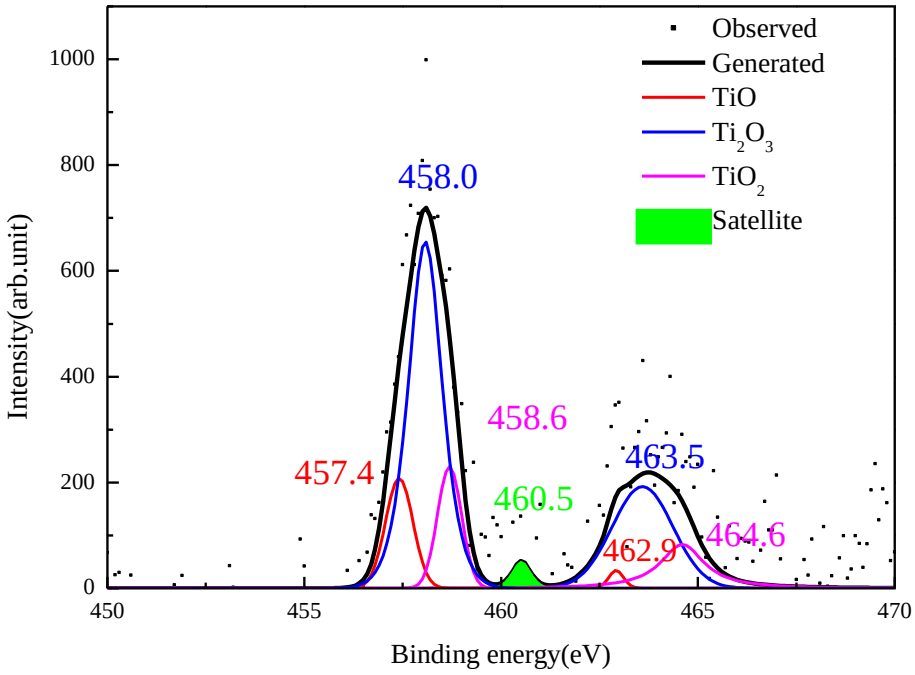

Fig. 8. (b)

Fig. 8. Measured Ti 2p peaks and deconvolution peaks of 3wt% impregnated LSTM on (a) Ni (E) / 8YSZ and (b) Ni (R) / 8YSZ substrates.

Table 3. Binding energy (BE) and % area of the Ti 2p peaks, obtained from the XPS analysis of various samples.

	BE peak shift (eV)						***Area %***						Ti^{3+}/Ti^{4+}	***Ti Charge***
	TiO (2+)		**Ti_2O_3 (3+)**		**TiO_2 (4+)**		**TiO (2+)**		**Ti_2O_3 (3+)**		**TiO_2 (4+)**			
	$2p_{3/2}$	$2p_{1/2}$	$2p_{3/2}$	$2p_{1/2}$	$2p_{3/2}$	$2p_{1/2}$	$2p_{3/2}$	$2p_{1/2}$	$2p_{3/2}$	$2p_{1/2}$	$2p_{3/2}$	$2p_{1/2}$		
LSTM -heat treatment under air atmosphere	457.1	462.3	457.5	463.3	458.1	463.8	3.09	5.10	30.90	11.0	38.56	11.35	0.84	3.42
LSTM -heat treatment under reducing atmosphere	457.4	463.0	457.8	463.6	458.5	464.3	1.72	9.21	36.14	9.80	31.52	11.61	1.07	3.32
LSTM (3wt%) -Ni (E) / 8YSZ	457.1	462.7	457.6	463.3	458.1	464.1	10.02	11.42	30.09	11.70	28.61	8.16	1.14	3.15
LSTM (3wt%) -Ni (R) / 8YSZ	457.4	462.9	458.0	463.5	458.6	464.6	10.99	0.98	45.48	22.54	10.65	9.36	3.40	3.10

3.8. Electrical conductivity under CH_4 condition

Electrical conductivities were measured in a dry CH_4 atmosphere using 3 wt% impregnated LSTM specimen on both substrates Ni (E) / 8YSZ and Ni (R) / 8YSZ. These two samples were chosen for the methane experiment because they showed the highest electrical conductivity properties under dry H_2 condition due to the fact that 3wt % impregnated LSTMs were effectively coating the surface and cross section of the substrates.

From the results shown as Fig. 9, the electrical conductivities of the LSTM (3wt%)-Ni (R) / 8YSZ sample showed higher values than those of the LSTM (3wt%)-Ni (E) / 8YSZ sample at all measured temperature ranges and it can be found that the difference in conductivity between them at relatively low temperatures is greater than at high temperatures. Significantly, the electrical conductivity of LSTM (3wt%)-Ni (E) / 8YSZ shows a rapid decrease from 750 °C. However, LSTM (3wt%)-Ni (R) / 8YSZ exhibits a relatively higher electrical conductivity, which implies that impregnated LSTM combined with a Ni (R) / 8YSZ substrate shows good resistance against carbon deposition under dry methane condition.

Summarizing these trends, the additional step of Ni removal from the surface of the Ni (E) / 8YSZ cermet before LSTM impregnation leads to the development of

resistance against carbon deposition as well as to a general improvement of electrical conductivity when used as a SOFC anode fueled by CH_4.

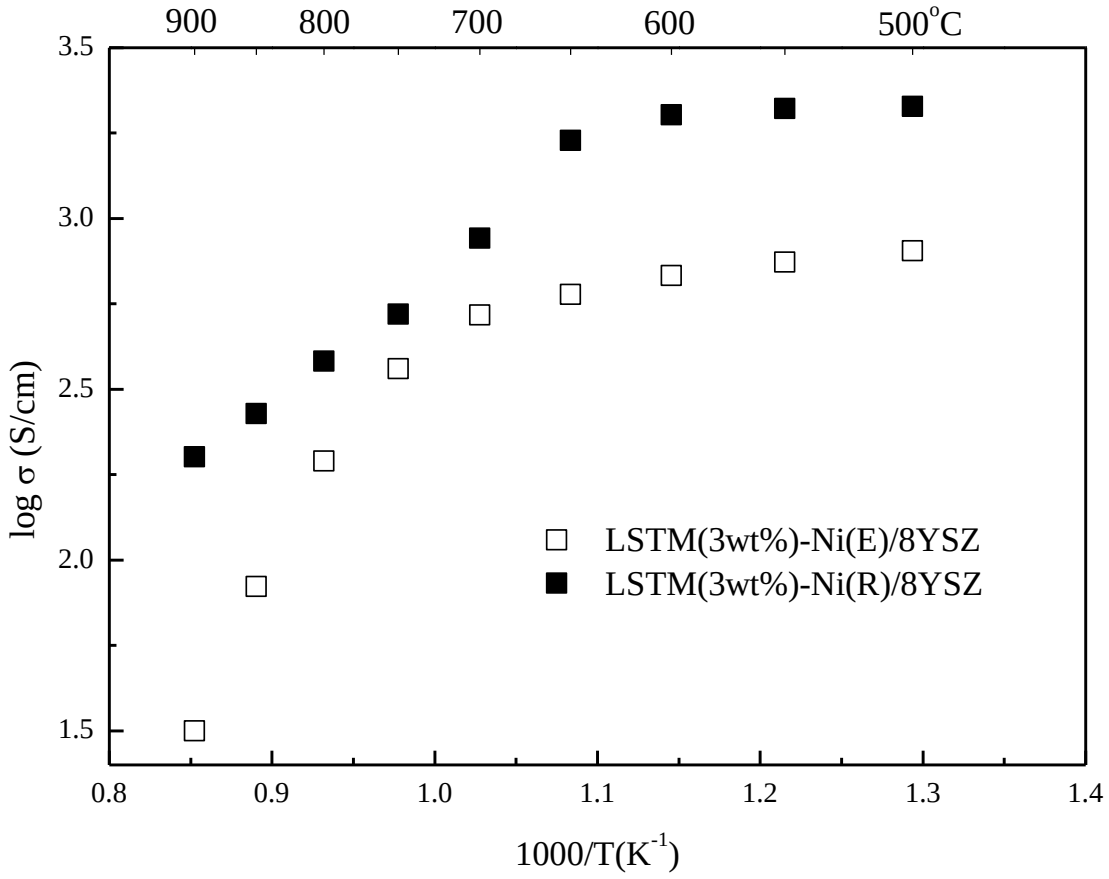

Fig. 9

Fig. 9. Summarized electrical conductivities of (a) LSTM (3wt%)-Ni (E) / 8YSZ and (b) LSTM (3wt%)-Ni (R) / 8YSZ under dry CH_4.

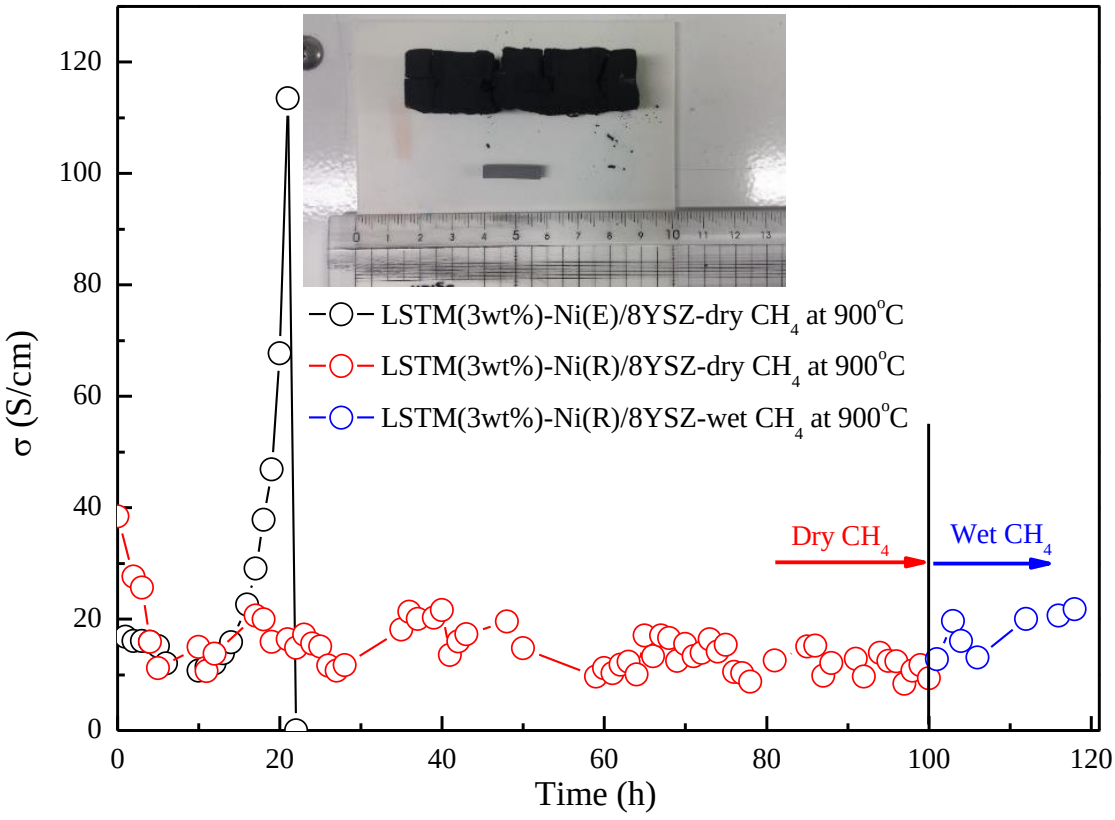

Fig. 10. Changes in electrical conductivity with time of LSTM (3wt%)-Ni (E) / 8YSZ and LSTM (3wt%)-Ni (R) / 8YSZ exposed to dry and wet CH_4 at 900°C.

Fig. 10 summarizes the electrical conductivity results of two samples, LSTM (3wt%)-Ni (E) / 8YSZ and LSTM (3wt%)-Ni (R) / 8YSZ, exposed to dry and wet CH_4 at 900°C. The electrical conductivity of LSTM (3wt%)-Ni (E) / 8YSZ was 16.8 S/cm initially in the first stage (h=0) of measurement at 900 °C, this value decreased with measuring time and then the value of electrical conductivity was 10.8 S/cm when exposed to dry

CH_4 after 10 hours. It can be seen that the conductivity increases rapidly after 10 hours due to the carbons deposited on the surface of the sample. After 20 hours, the maximum electrical conductivity value of 113.5 S/cm was shown and then it was impossible to measure the conductivity of LSTM (3wt%)-Ni (E) / 8YSZ sample any more with a rapid decrease because carbons existing on the surface infiltrated the inside of the support, a rapid volume expansion occurred as can be seen from the change in the shape of the sample included as an inset in Fig. 10.

However, the LSTM (3wt%)-Ni (R) / 8YSZ sample showed an average electrical conductivity value of about 19S/cm up to 100 hours and maintained in a stable state for a long time under dry CH_4 condition at 900 ^oC. When measured in a wet CH_4 atmosphere for 20 hours after 100 hours, the electrical conductivity was slightly increased while maintaining an average value of about 21 S/cm.

Fig. 11 shows the microstructural characteristics of LSTM (3wt%)-Ni (E) / 8YSZ and LSTM (3wt%)-Ni (R) / 8YSZ samples on the surface after the end of the experiments shown as Fig. 10. Fig. 11 (a) shows the top view of LSTM (3wt%)-Ni (E) / 8YSZ after supplying dry CH_4 for 21 hours and Fig. 11 (b) shows the top view of LSTM (3wt%)-Ni (R) / 8YSZ after supplying dry CH_4 for 100 hours and then supplying wet CH_4 for 20 hours.

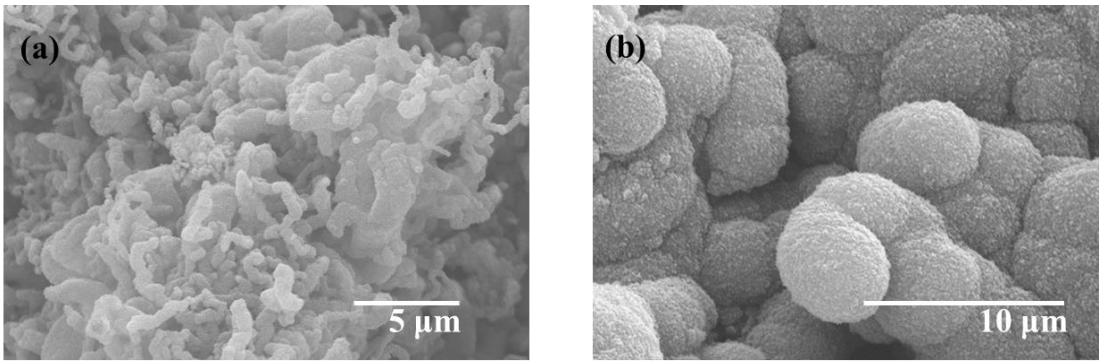

Fig. 11. SEM images of the (a) LSTM (3wt%)-Ni (E) / 8YSZ and (b) LSTM (3wt%)-Ni (R) / 8YSZ exposed to dry and wet CH_4 at 900°C after completion of electrical conductivity measurement.

Clear microstructural distinction in the surfaces of two samples can be directly observed in Fig. 11. For example, carbon fibers on the surface of LSTM (3wt%)-Ni (E) / 8YSZ samples were generated [22], which indicates that the carbon deposition resulted in short-term destruction of the anode structure in Fig. 11 (a). However, in the case of the LSTM (3wt%)-Ni (R) / 8YSZ sample in which the LSTM was impregnated on the 8YSZ surface by removing Ni in Fig. 11 (b), although spherical carbons were deposited, the structures maintaining the surface network remained intact. Due to the difference in the morphology of decomposition particles, not only the shape and size of the LSTM (3wt%)-Ni (R) / 8YSZ sample could be maintained, but also a constant conductivity

could be maintained. The impregnation of LSTM into a Ni/8YSZ cermet after removing Ni from its surface leads to a significant change in microstructure of the sample compared to a sample in which the same LSTM impregnation was performed into a Ni / 8YSZ cermet without Ni removal. Effects of this microstructural change under conditions experienced if used as a SOFC anode, like improvement of the electrical conductivity performance as well as resistance to carbon deposition on its surface could be confirmed.

4. Conclusions

In this research, the microstructural and electrochemical properties of samples of LSTM impregnated Ni (E) / 8YSZ and Ni (R) / 8YSZ substrates were investigated aiming at the application as anode material for SOFCs.

When reduced Ni (R) / 8YSZ substrates were exposed to the acid solution, Ni was easily eluted at the first measurement period (from 0 to 5 minutes) with rate of 3.32 wt%/min and then the amount of Ni removed showed a low dissolution rate of 2.29 x 10^{-2} wt%/min.

Investigation of the microstructure of LSTM on a Ni (R) / 8YSZ substrate showed that LSTM was uniformly distributed on the grain and formed a structure LSTM particles serially connected in the form of particle chains from an impregnation level as low as 3 wt% on top of the Ni (R) / 8YSZ substrates.

Electrical conductivity values of samples with LSTM impregnated onto a Ni (E) / 8YSZ substrate proof to be lower than those of samples with LSTM impregnated onto a Ni (R) /8YSZ substrate and the values of LSTM impregnated onto Ni (R) / 8YSZ were surprisingly even much higher than those of the pure Ni (E) / 8YSZ sample. These higher conductivities of samples of LSTM impregnated onto a Ni (R) / 8YSZ substrate are caused by the presence of metallic Ti at the grain boundaries, which can be observed by EDS analysis. Additional proof for the existence of metallic Ti at the grain boundaries of these reduced samples was provided by XPS results showing a satellite peak at bounding energy values related to Ti^0 in literature. In summary, the existence of Ti caused by the reduction of impregnated LSTM can only be observed if LSTM is impregnated onto a substrate with a Ni free surface, meaning a surface from which Ni has been eluted in the way described above fabricating Ni (R) / 8YSZ. The existence of metallic titanium can lead to improved electrical conductivity.

Finally, LSTM (3wt%)-Ni (R) / 8YSZ showed electrical conductivity values which

were higher than those of LSTM (3wt%)-Ni (E) / 8YSZ in all the temperature ranges when measured under dry CH_4 atmosphere.

Acknowledgments

The authors are grateful for the support of the Basic Science Research Program through the National Research Foundation of Korea (NRF), funded by the Ministry of Science, ICT & Future Planning (No. 2014R1A1A1004163) and the National Research Foundation of Korea (NRF) grant funded by the Korea government (MSIT) (No. 2019R1A2C1087534). This research was also supported by the research fund of Hanbat National University in 2019.

References

[1] J. Mermelstein, M. Millan, N. P. Brandon, The impact of carbon formation on Ni-YSZ anodes from biomass gasification model tars operating in dry conditions, Chem. Eng. Sci. 64 (2009) 492-500.

[2] J. Kong, K. Sun, D. Zhou, N. Zhang, J. Mu, J. Qiao, Ni-YSZ gradient anodes for anode-supported SOFCs, J. Power Sources, 166 (2007) 337-342.

[3] Y. Jin, H. Yasutake, K. Yamahara, M. Ihara, Improved electrochemical properties of Ni/YSZ anodes infiltrated by proton conductor SZY in solid oxide fuel cells with dry methane fuel: Dependence on amount of SZY, Chem. Eng. Sci. 65 (2010) 597-602.

[4] W. Bao, Q. Chang, G. Meng, Effect of NiO/YSZ compositions on the co-sintering process of anode-supported fuel cell, J. Membrane Sci. 259 (2005) 103-109.

[5] M. Pihlatie, A. Kaiser, M. Mogensen, Redox stability of SOFC: Thermal analysis of Ni–YSZ composites, Solid State Ionics, 180 (2009) 1100-1112.

[6] E. Ivers-Tiffée, A. V. Virkar, Electrode polarisations, Chapter 9 in High temperature solid oxide fuel cells: Fundamental, design and applications, edited by S. C. Singhal, K. Kendall, Elsevier, Kidlington, UK, 2003.

[7] R. J. Gorte, J. M. Vohs, S. McIntosh, Recent developments on anodes for direct fuel utilization in SOFC, Solid State Ionics 175 (2004) 1-6.

[8] W. Zhu, C. R. Xia, J. Fan, R. R. Peng, G. Y. Meng, Ceria coated Ni as anodes for direct utilization of methane in low-temperature solid oxide fuel cells, J. Power Sources 160 (2006) 897-902.

[9] S. I. Lee, J. M. Vohs, R. J. Gorte, A Study of SOFC Anodes Based on Cu-Ni and Cu-Co Bimetallics in CeO_2 - YSZ, J. Electrochem. Soc. 151 (2004) A1319-A1323.

[10] Z. Xie, C. R. Xia, M. Y. Zhang, W. Zhu, H. T. Wang, $Ni_{1-x}Cu_x$ alloy-based anodes for low-temperature solid oxide fuel cells with biomass-produced gas as fuel, J. Power Sources 161 (2006) 1056-1061.

[11] H. Kim, C. Lu, W. L. Worrell, J. M. Vohs, R. J. Gorte, Cu-Ni Cermet Anodes for Direct Oxidation of Methane in Solid-Oxide Fuel Cells, J. Electrochem. Soc. 149 (2002) A247-A250.

[12] E. W. Park, H. Moon, M. S. Park, S. H. Hyun, Fabrication and characterization of Cu–Ni–YSZ SOFC anodes for direct use of methane via Cu-electroplating, Int. J. Hydrog. Energy 34 (2009) 5537-5545.

[13] Z. C. Wang, W. J. Weng, K. Cheng, P. Du, G. Shen, G. R. Han, Catalytic modification of Ni–Sm-doped ceria anodes with copper for direct utilization of dry methane in low-temperature solid oxide fuel cells, J. Power Sources 179 (2008) 541-546.

[14] J. H. Kim, D. Miller, H. Schlegl, D. McGrouther, J. T. S. Irvine, Investigation of microstructural and electrochemical Properties of Impregnated (La,Sr)(Ti,Mn)$O_{3\pm\delta}$ as a potential anode material in high-temperature solid oxide fuel cells, Chem. Mater. 23 (2011) 3841-3847.

[15] K. Kim, J. Jeong, A. K. Azad, S. B. Jin, J. H. Kim, X-ray photoelectron spectroscopic study of direct reforming catalysts $Ln_{0.5}Sr_{0.5}Ti_{0.5}Mn_{0.5}O_{3\pm d}$ (Ln = La, Nd, and Sm) for high temperature-operating solid oxide fuel cell, Appl. Surf. Sci. 365 (2016) 38-46.

[16] Y. -H. Joung, H. I. Kang, W. S. Choi, J. H. Kim, Investigation of x-ray photoelectron spectroscopy and electrical conductivity properties of the layered perovskite $LnBaCo_2O_{5+d}$ (Ln = Pr, Nd, Sm, and Gd) for IT-SOFC, Electron. Mater. Lett. 9 (2013) 463-465.

[17] J. H. Kim, X-ray photoelectron spectroscopy analysis of $(Ln_{1-x}Sr_x)CoO_{3-\delta}$ (Ln: Pr, Nd and Sm), Appl. Surf. Sci. 258 (2011) 350-355.

[18] Y. Kim, H. Schlegl, K. Kim, J. T.S. Irvine, J. H. Kim, X-ray photoelectron spectroscopy of Sm-doped layered perovskite for intermediate temperature-operating solid oxide fuel cell, Appl. Surf. Sci. 288 (2014) 695-701.

[19] M. K. Rath, B.-G. Ahn, B.-H. Choi, M.-J. Ji, K.-T. Lee, Effects of manganese

substitution at the B-site of lanthanum-rich strontium titanate anodes on fuel cell performance and catalytic activity, Ceram. Int. 39 (2013) 6343-6353.

[20] V. R. Mastelaro, P. N. Lisboa-Filho, P. P. Neves, W. H. Schreiner, P. A.P. Nascente, J. A. Eiras, X-ray photoelectron spectroscopy study on sintered $Pb_{1-x}La_xTiO_3$ ferroelectric ceramics, J. Electron. Spectrosc. Relat. Phenom. 156-158 (2007) 476-481.

[21] M. Viviani, M.T. Buscaglia, P. Nanni, R. Parodi, G. Gemme, A. Dacca , XPS investigation of surface properties of $Ba_{(1-x)}Sr_xTiO_3$ powders prepared by low temperature aqueous synthesis, J. Eur. Ceram. Soc. 19 (1999) 1047-1051.

[22] K. Cheng, H. Chen, W. Weng, C. Song, P. Du, G. Shen, G. Han, Effects of dual Cu incorporation on carbon deposition in SDC anode, J. Alloys and Compd. 541 (2012) 65-69.